Polish Journal of Chemical Technology, 19, 1, 132—142, 10.1515/pjct-2016-0050

Improving heat aging and mechanical properties of fluoroelastomer using carbon nanotubes

Javad Heidarian[1, 2*], Aziz Hassan[1]

[1]*University of Malaya, Polymer and Composite Materials Research Laboratory, Department of Chemistry, 50603, Kuala Lumpur, Malaysia*
[2]*Nanotechnology Research Center, Research Institute of Petroleum Industry(RIPI)-West side of Azadi Complex-Tehran--Iran, 1485733111*
[*]*Corresponding author: e-mail: heidarianj@um.edu.my, heidarianj@yahoo.com*

Carbon nanotube (CNT)-, carbon black (CB)-filled fluoroelastomer (FE) and unfilled-FE compounds were prepared (CNT/FE, CB/FE and FE). The compounds were subjected to heat air aging and characterized by tensile test and X-Ray Diffraction (XRD) analysis. Results show that CNT improved tensile properties of FE before and after aging. All samples show stress induced crystallization (SIC) during tension. XRD results show that under all conditions, the crystals were in the form of γ-phase. For both aged and un-aged specimens, the degree of crystallinity (X_c) is low. After tensile stretching, X_c of un-aged specimens increases tremendously, with larger crystal size. Under the same conditions, the order of elongation at break (EL) was FE > CB/FE > CNT/FE. Normal modulus (NM) and tangent modulus (TM) at the same conditions was in the order of CNT/FE > CB/FE > FE. Tensile strength had the order of CNT/FE > CB/FE > FE.

Keywords: fluoroelastomers, crystallization, tension test, X-ray diffraction topography, aging.

INTRODUCTION

Carbon nanotubes (CNT) can improve many properties of fluoroelastomers (FE) for different applications especially in oil and gas industries[1–3]. To predict the service life of a rubber component subjected to a variety of environments, it is necessary to account for all modes of degradation. CNT is expected to improve aging and mechanical properties of FE compared to unfilled FE or carbon black (CB) filled FE (CB/FE).

Faulkner et al.[4] reported on improving tensile and tear strength and energy to break (elongational stress--strain energy to failure) in CNT/FE nanocomposites. The authors concluded that CNT at low durometer in peroxide cure FE compared to CB/FE is not effectively reinforcing. However, CNT highly reinforces FE at high durometer/stiffness. Changes in mechanical properties of CNT/FE due to heat aging were also reported.

Wang et al.[5] verified the aging behavior of the reactive blends of FE and another nitrile or natural rubber. The authors used fourier transform infra-red (FTIR) spectroscopy and X-ray photoelectron spectroscopy (XPS) for the characterization. Their results showed that FE underwent thermal oxidation and hydrofluorination reaction during aging. Subsequently carboxyl group and carbon double bond were formed, and fluoro group shifted to the surface at the aging temperature of 200°C.

A considerable depletion of fluorine (F) and carbon (C) on the surface and to the depth of around 10–15 μm of cross-section of aged CB/FE seals in oil containing amine based dispersant at 150°C was also reported by Smith et al.[6] The authors concluded that polytetrafluoroethylene (PTFE) begins to soften and release F at around 200–220°C. This may explain the apparent susceptibility to heating in air shown by elastomer with high tetra-fluoroethylene (TFE) content.

Change in crystallinity of filled fluoropolymers under shear is reported by many researchers[7–9]. Chae and Hong[10] reported that in the dynamic crystallization under shear, MWCNTs have a nucleating effect on the PVDF, reducing both induction and crystallization times with increasing MWCNT contents. The same phenomenon for PVDF-nanoclay composites was reported by Yang et al.[11]. According to this study, shear field and organophilic montmorillonite (OMMT) nanoclay synergistically promote the formation of polar crystalline phase (β- or γ-crystalline phase with trans-conformers) in PVDF. On the other hand, it was reported that external force fields, such as ultrasonication[12], uniaxial stretching and electric field (electrospinning)[13–15], are helpful for overcoming the energy barrier of molecular chain configuration, thus facilitating the formation of polar crystalline phase in PVDF.

Effects of CNT on improving tensile properties of FE before and during heat air aging are seldom verified by researchers. As such, comparisons of tensile properties of CNT/FE with CB/FE and FE in the above conditions are yet to be carried out. FE, CB/FE and CNT/FE specimens were subjected to the degree of crystallinity characterization by XRD analysis. Comparisons were made between before and after aging (original compound) and before and after tensile test of un-aged, tensile fractured specimens. Comparisons between the tensile tested aged- and un-aged specimens were also made. Analyses in these aspects are rather novel, specifically verifying the possible stress induced crystallization (SIC) in the tensile tested samples. These findings will show the possible potential of CNT in improving tensile properties and aging resistance of CNT/FE compared to CB/FE and FE. This improvement of crystallinity consequently will improve tensile properties of CNT/FE compared to CB/FE and FE.

EXPERIMENTAL

Material

Materials used were Viton GF-600S fluoroelastomer, FE, a terpolymer of hexafluoro-propylene (HFP), vinyli-

dene fluoride (VDF), and TFE with a cure site monomer; organic peroxide, Luperox 101 XL-45; carbon nanotube, CNT (TNM8, outside diameter > 50 nm, purity > 95%, and length of 10–20 μm); carbon black, CB Ensaco 250; and triallylisocyanurate, TAIC supplied by ERIKS Sdn. Bhd. (Malaysia), Arkema Sdn. Bhd. (Malaysia), Chengdu Organic Chemicals Co. Ltd. (Chinese Academy of Sciences, China), Age D'Or Industrial Sdn. Bhd. (Malaysia) and Liu Yang San Ji Chemical Trade Co. Ltd. (China) respectively. Three formulations were compounded; CNT filled FE (CNT/FE), CB filled FE (CB/FE) and unfilled FE (FE). In all compounds, the amount of FE, organic peroxide and TAIC were 70.0, 2.1 and 2.1 g respectively. For CNT/FE and CB/FE, 7.0 g of CNT and CB respectively, were added.

Compounding

Mixing FE with additives was done using a laboratory scale two roll mill with a roll temperature of 48°C. FE in the above mentioned composition was supplied to open roll. A uniform band was formed while three rolling cuts from each side of the mill were made, so that the polymer becomes homogenous and sufficiently warm up. Then TAIC was added uniformly into the gum and three rolling cuts from each side of the mill were done. After setting the roll distance to 1.1 mm, CNT was then fed in. The compound was then tight milled ten times. The roll distance was then adjusted to 1.1 mm, and peroxide was added. Once the final 5 to 6 rolled up end passes, the mixture was supplied to the open roll and sheeted. After 24 hours, re-milling was done with a roll temperature of 26°C. The same procedure was used for CB/FE and FE.

Curing and post curing

Curing of FE compound was done with the mold (18 cm × 18 cm × 2 mm) in a heated press, at 177°C under pressure of 10 MPa for 7 min. The post curing was done in air oven at 232°C for 2 hours. Conditions for curing and post curing were recommended by the supplier.

Thermal aging

Thermal aging was done according to ASTM D-573 standard for 24, 48 and 72 hours at 250°C. The samples were named FE, FE-24, FE-48 and FE-72, where the numbers following, FE indicates the aging time in hours. Similar styles of abbreviations were used for CB/FE and CNT/FE aged samples.

Characterization

Tensile test The dumb-bell shaped specimens were cut from the molded post-cured rubber sheet using Wallace (UK) type C die cutter. Tensile properties were determined according to ASTM D-412 standard at room temperature using universal testing machine, Instron 3345 (USA) with load-cell of 5 kN and the cross-head speed of 500 mm min^{-1}. Minimum of six specimens were tested and the data reported is the average of at least four reproducible results.

X-Ray Diffraction (XRD) Un-aged and aged samples of 1.5 cm × 1.5 cm × 2.0 mm dimensions from the molded post cured FE, CB/FE and CNT/FE rubber sheets were used for XRD analyses. The fractured tensile specimens of aged and un-aged samples were also characterized. For these tests, samples were cut from the near broken area of the dumb-bell specimens. The samples were named with additional 'T' at the end of original name, for instance FE-72T, in which T indicates that the sample was taken from the broken specimen of tensile test. The same abbreviations were used for other samples. XRD spectrometer, PANalytical Empyrean Model DY1032 was used for the characterization at 2θ of 5° to 80°.

RESULTS AND DISCUSSION

Tensile properties

Figure 1 (a) shows the selected stress-strain curves for un-aged and 72 hours aged FE composites. Their properties are discussed individually below.

Tensile strength Figure 1 (b) shows the tensile strength (TS) of FE composites at different aging times, extracted from the stress-strain curves. As can be seen from this figure, TS of FE and CB/FE decrease with increasing aging time (except during the first 24 hours). However, for CNT/FE; TS has negligible decreases with increasing aging time (except during the first 24 hours). In CNT/FE, most degradation happened during the first 24 hours and not much change after that. However, for CB/FE and FE degradation continued until 72 hours. This is due to better degradation resistance of CNT.

TS of FE and CB/FE increases after 24 hours of aging compared to un-aged FE and CB/FE respectively (probably due to increase in cross-linking).

Elongation at break (EB) Figure 1 (c) shows the elongation at break (EB) of FE composites at different aging times. Normally, the change in EB due to aging is a criterion of degradation, therefore less change in EB show less effect of aging. As can be seen in this figure, EB for FE and CB/FE increases with increasing aging time during the first 24 hours however, with further increasing the aging time the changes in EB are negligible. In comparison to CNT/FE, EB of CNT/FE-24 decreases slightly after 24 hours of aging. However, after 48 hours, EB increases while until 72 hours it is almost constant. This behavior proves that most of CNT/FE degradation happened during the first 48 hours.

Comparing tensile strength and elongation at break of un-aged specimens As can be seen in Figure 1 (a–c), among all samples, FE has the highest EB and the lowest TS, and CNT/FE has the highest TS and lowest EB, while CB/FE has intermediate EB and TS. However, in comparing CNT/FE and CB/FE curves, it shows that CNT improves TS and increases EB. This is because CNT is nanofiller which have more surface area compared to normal filler of CB. More surface area will cause more interaction between CNT and FE compared to CB and FE. Thus, it causes more physical and chemical contact resulting in more cross-linking points and less free volume[1, 16, 17]. Therefore, CNT/FE has higher TS and lower EB. Pham et al.[16] also studied the effect of increasing CNT loadings on the mechanical properties such as tensile strength, tensile modulus, elongation at break, hardness and tear resistance. The authors concluded that

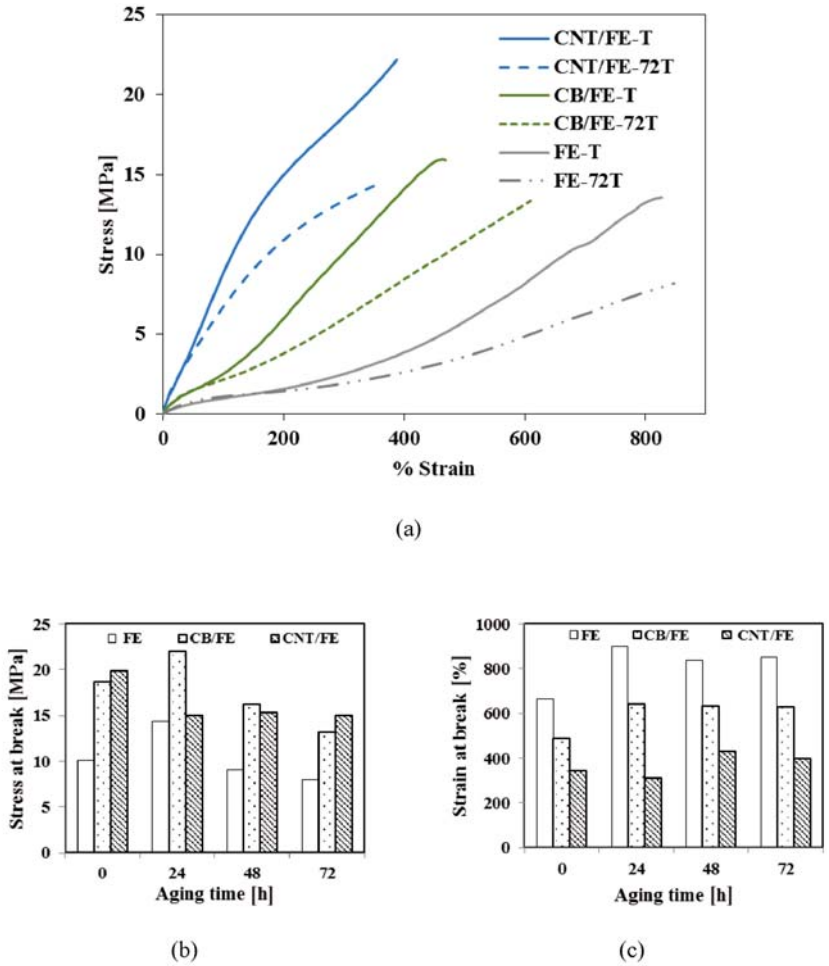

Figure 1. (a) Stress-strain curves of unaged and 72 hours aged samples, (b) Tensile strength and (c) Elongation at break at different aging times of filled and unfilled FE

a continuous increase in the performance characteristics shows the reinforcing nature of CNT in FE.

Stress induced crystallization (SIC) Figure 1 (a) also shows that FE undergo stress hardening or stress induced crystallization (SIC), that starts at about 200% strain. SIC will cause increase in modulus and strength. The SIC is very similar to necking phenomenon in polymer. The same phenomenon can be seen in CB/FE whereby SIC starting at about 100% strain. Thus in CB/FE, SIC starts from lower strain. This is due to having less necking strain domain in the case of CB/FE, caused by the interaction between filler and FE which resulted in more physical and chemical bonds acting as cross-linking points for FE. These cross-linking points inhibit the chains of polymers from slipping and therefore resulting in shorter strain range in which crystallization happened. Upon stretching, γ-phase of VDF crystals is formed. Producing γ-phase in VDF segments needs a high shear which can be obtained upon using high strain[10].

For CNT/FE, SIC appeared at 50% strain. This is again due to more cross-linking points between CNT and FE with less free volume compared to CB/FE as explained previously. Figure 1 (a) also shows that the tangent modulus of FE and CB/FE increases with increasing strain. On the other hand, tangent modulus of CNT/FE at strains above 100% decreases with an increase in strain.

Figure 1 (a) also shows that, SIC for 72 hours aged FE and CB/FE started at the same strain as the un-aged samples. This clearly indicates that aging does not affect the SIC initiation in FE and CB/FE.

Tangent modulus Figure 2 (a–c) show the tangent modulus versus strain of unfilled and filled FE at different aging times. As can be seen in Figure 2 (a), for FE and aged FE the tangent modulus decreases from 0% to 200% strain and at strains higher than 200% it increases with increasing strain. This explains that in FE and aged FE, the SIC starts from 200% strain. This FE containing VDF and TFE segments are capable of producing crystals particularly under shear fields[10, 18]. Figure 2 (b) indicates that for both aged and un-aged CB/FE, the minimum tangent modulus appears at around 100% strain (SIC starting point). In comparison, SIC of aged and un-aged CB/FE and FE reached at much lower strains.

Figure 2 (c) shows that for CNT/FE, a minimum tangent modulus at around 50% strain in the strain range of 0–100% and at strains higher than 100%, there is a continuous decrease in modulus. The continuous decrease in tangent modulus happens (occurs) when deformation (strain) is increased, because some of the physical cross-linking may dissipate as polymer chain slides over the nanotube resulting in the deterioration of properties. The similar deterioration in properties with deformation was explained for CNT-natural rubber nanocomposites[17].

As can be seen from Figure 2 (a–c), at each fixed strain the modulus of unfilled and filled -FE decreases

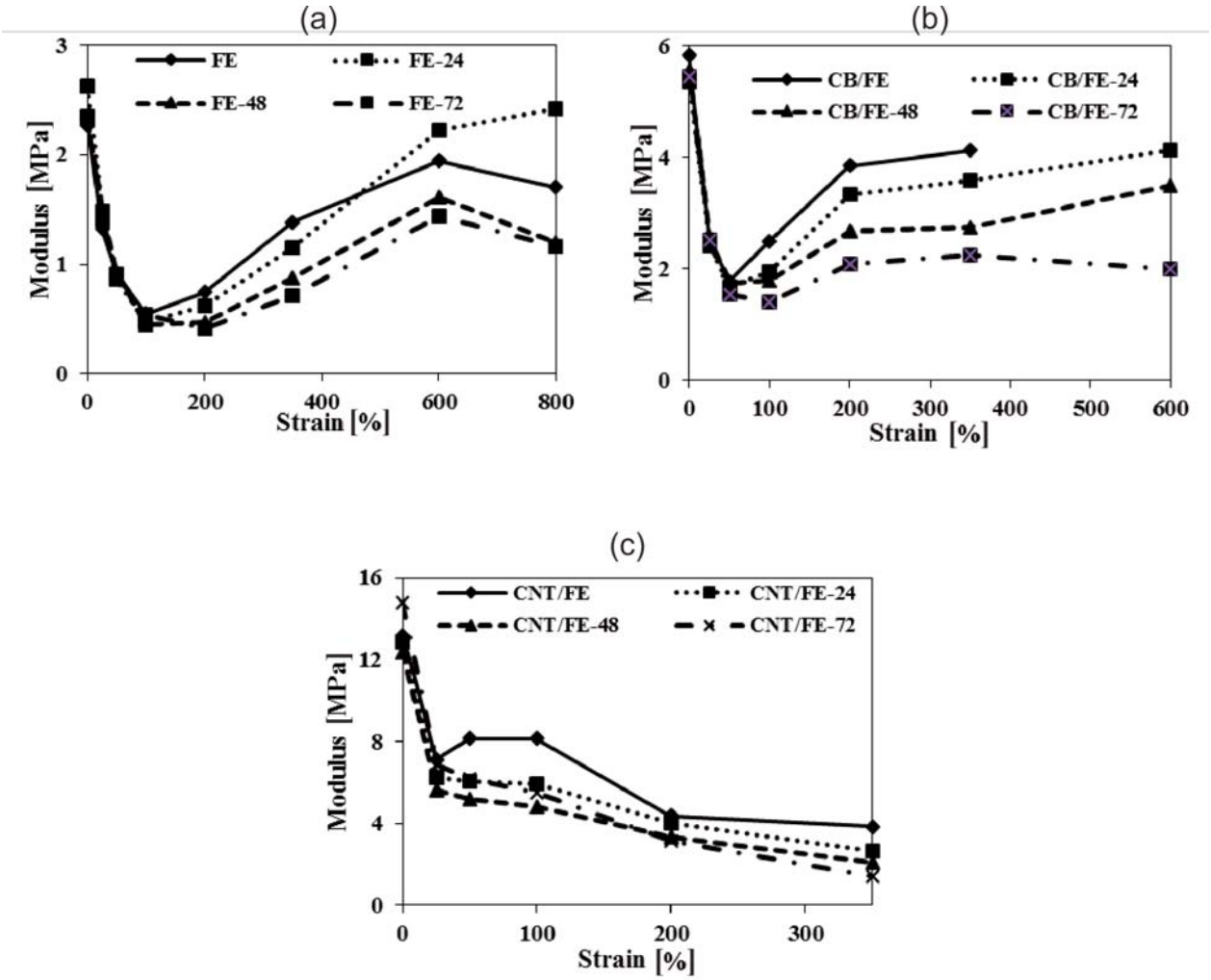

Figure 2. Tangent modulus versus strain of: (a) FE, (b) CB/FE and (c) CNT/FE at different aging times

with increasing aging time. This is due to the increasing degradation and reducing crystallinity of them after aging. Figure 2 (c) also shows that for CNT/FE, the most significant change in tangent modulus at each fixed strain is during the first 24 hours of aging.

Higher shear due to the presence of CNT and more physical and chemical cross-links between CNT and FE causes SIC to appear at lower strains compared to CB/FE and FE. The same reasons can be attributed for SIC in CB/FE starting at lower strains compared to that of FE.

Figure 3 shows the tangent modulus ratio (TMR) of FE composites at different aging times, defined as,

$$TMR_{s1,s2} = \frac{TM_{s1}}{TM_{s2}} \quad (1)$$

where, $TM_{\varepsilon 1}$ and $TM_{\varepsilon 2}$ are the tangent moduli at strains 1 and 2 respectively.

The above ratio is obtained by dividing tangent modulus at a strain after SIC has started ($TM_{\varepsilon 1}$) by the tangent modulus at a strain before ($TM_{\varepsilon 2}$). These ratios were obtained in order to see how SIC improve the tensile properties. For FE, for example $TM_{600,100}$ was used, for CB/FE, $TM_{350,50}$ and for CNT/FE, $TM_{100,25}$ and $TM_{350,250}$ were chosen. As shown in Figure 3, the ratios are greater than 1, indicating high SIC. The ratio larger than 1 (horizontal line at TMR = 1) shows increase in modulus and indicates SIC. The TMR for CNT/FE is almost 1. This is because the tangent moduli of CNT/FE before SIC are already high and SIC slightly improves the tangent modulus. The ratios have the following order for different fillers at each aging time: FE > CB/FE > CNT/FE. This shows more improvement in the moduli of FE under shear compared to the others.

Figure 3 also shows that for all samples, the ratio reduces with increasing aging time. This is because of decrease in percentage of crystallinity due to degradation, dehydrofluorination and carbon oxygen reactions, particularly at and near the surface[5], therefore reducing the modulus of elasticity.

Normal modulus Figure 4 shows the normal modulus (NM) of FE composites at different aging times and strains. NM is the stress obtained from tensile stress--strain curves at a fixed strain. For example, NM100 is the stress at 100% strain of tensile test curve. The results in Figure 4 shows that at each fixed strain, NM decreases in the order of CNT/FE > CB/FE > FE. The reasons for improvement in tensile properties in the above order are the same reasons as explained for the TS. Results indicate that NM mostly decreases with increasing aging time especially at higher strains; however, there was no fixed trend at lower strains. The reasons for the decrease in NM with aging time are the same as explained for TM reduction with aging time.

At high strains, the effect of degradation is significant because of shorter polymer chains in the aged samples. It is due to thermal and oxidative degradation as well as low percentage of crystallinity in them as explained before.

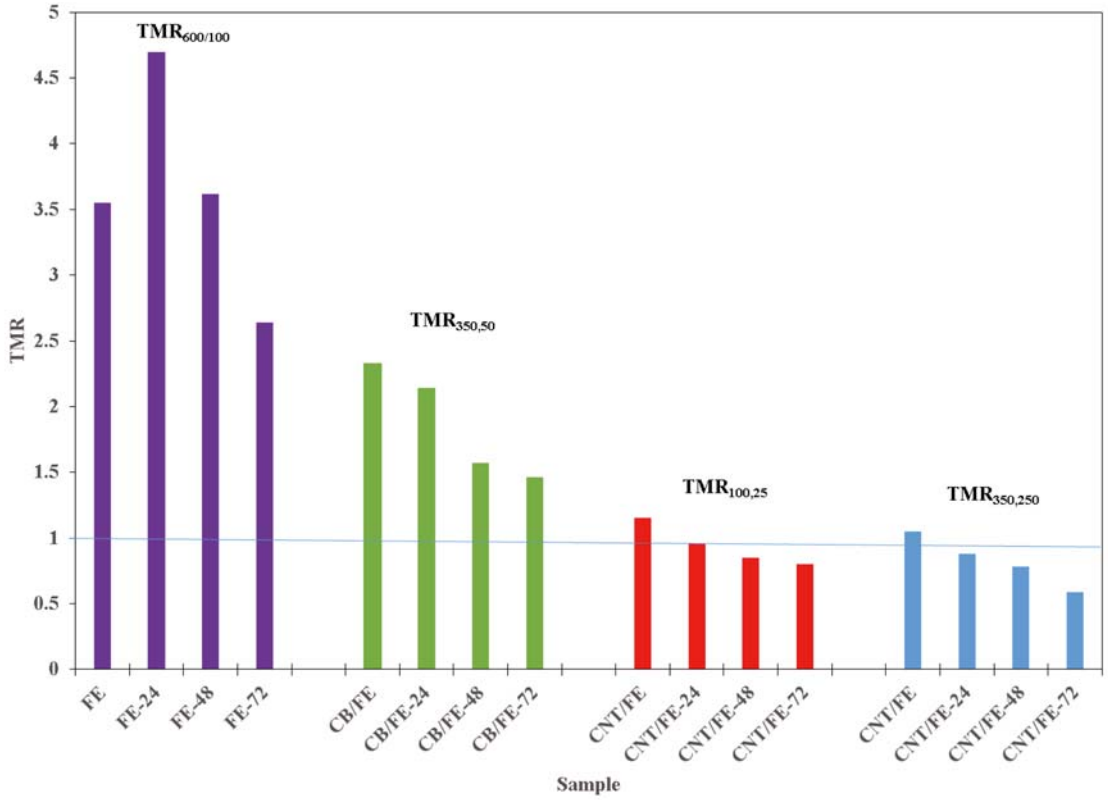

Figure 3. Tangent modulus ratio (TMR) of filled- and unfilled-FE at different aging times

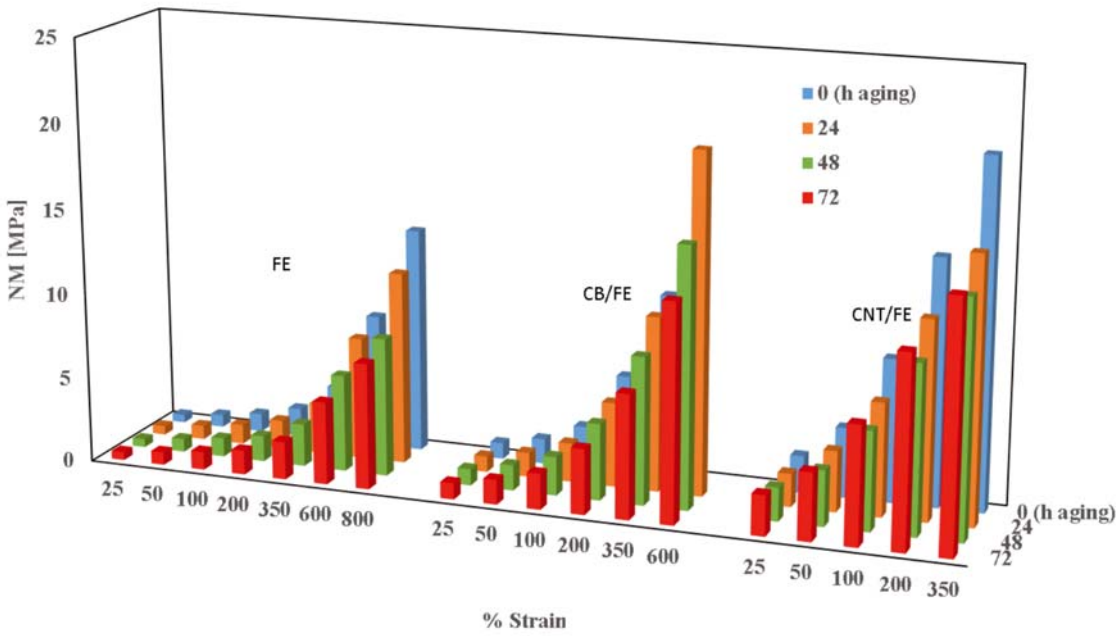

Figure 4. Normal modulus (NM) of filled- and unfilled-FE at different aging times and strains

For CB/FE composites, at lower strains the NM is almost constant. This indicates that CB can prevent degradation at low deformations. This is because under low strain, the physical cross-links between filler and FE is not dissipated. Under low deformation, filler is also the major component contributing to the composite properties. Bonded rubber to filler is also a contributing factor by increasing effective filler amount, resulting in reducing degradation.

For CNT/FE (Fig. 4), the same trend as CB/FE sample is observed. There is more dissipation of physical cross-linking between CNT and FE at high deformations compared to CB and FE, resulting in more drops in NM. The reasons are the same as explained for TM.

Totally it can be concluded that CNT improved tensile properties of FE before and after aging. CNT can prevent degradation of FE for several reasons. Firstly, the presence of CNT in FE makes the active centers of FE main chains inactive, preventing the degradation, therefore can preserve FE nearer to the CNT surface. Secondly, the interaction between CNT and FE results in increased physical and chemical cross-linking points

which prevent the degradation of the polymer chains. Considering that the degradation of FE is a radical chain reaction, it is therefore susceptible to inhibition by reagents capable of trapping such radicals. Furthermore, the antioxidant nature of CNT, attributed to its high electron affinity (≈ 2.65 eV), enables it to act as a radical scavenger. Consequently, CNT helps to trap radicals and inhibiting degradation of FE nearer to it. A similar reason has been given for increased decomposition temperature caused by using CNT in FE[16]. Moreover, Endo et al.[1], reasoned that thermal stability of FE near CNT is due to the presence of bounded rubber to CNT and concluded that this structure can prevent the decomposition of rubber at high temperatures by resisting the molecular mobility.

XRD

XRD of FE Figure 5 shows XRD spectra of FE and FE-72 before and after tensile test. The figure shows that for FE, there is a sharp peak at 2θ = 29.45° and some small peaks at 36.08°, 39.47°, 41.05° and 43.16°. All of these peaks belonged to γ-phase of VDF segments[18–23]. Particularly the peak at 29.45° belongs only to γ-phase[23]. Because the intensity of these peaks except the one at 29.45° is very low, therefore FE is only slightly crystalline. Table 1 shows the relative intensity, height, full width at half maximum (FWHM) and tip width of each peak for FE. The relative intensity is the ratio of the peak intensity to that of the most intense peak. Relative intensity can be used for comparing intensity of peaks to each other in one sample and to the similar peaks at another sample. Height of the peak is directly related to the peak intensity. FWHM is inversely related to the crystallite size. The tip width is the width, where the second derivative is less than zero. The smaller the FWHM value and tip width, the more homogeneous the grids and the more orderly arrangement of crystals are.

However, in the same figure for FE-T, it can be seen that almost the same peaks (having nearly the same intensity) as that of FE appeared. However, two new peaks at 14.46° and 28.72° appeared, again showing γ-phase crystallinity[19] of FE-T with slightly more crystallinity compared to FE. Table 1 also shows the peak list for FE-T. The peaks at 5.96° and 16.63° for FE and 6.64° and 16.73° for FE-T respectively contains amorphous hollows of FE and FE-T[24]. In FE-T, due to increasing crystallinity, the intensity of these two peaks decrease compared to that of FE respectively.

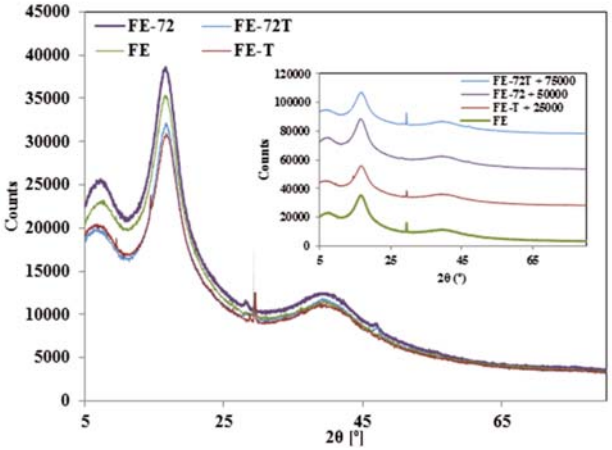

Figure 5. An XRD spectra of FE and FE-72 before and after tensile test (overlaid and separated)

The relative intensity in Table 1 is the intensity ratio of each peak to the amorphous peak at 16.63° for FE and FE-T. Therefore, increase in relative intensity of each common crystal peaks in FE-T compared to that of FE in that table shows that the crystallinity increases in FE-T. The reasons being, the intensity of crystalline peak increased and the amorphous peak intensity decreased as mentioned before, therefore the ratio of them (relative intensity) increased. As a result, the increase in relative intensity can be a criterion for comparing crystallinity between different samples. For the common peaks of FE and FE-T, FWHM and tip width also increased or remained unchanged. However, for new peaks in FE-T, FWHM and tip width are low, indicating that the size and order of crystals is high in FE-T. The above results and having new peaks in FE-T compared to FE shows that after tensile test, crystallinity increase due to SIC. These results also confirm the tensile results that showed SIC during tensile test for FE.

Figure 5 also shows that in FE-72, there are some main peaks at 28.17°, 39.35°, 39.26° and 46.66° and some small peaks at 42.12° and 55.52°. Once again, all of these peaks show γ-phase crystallinity of VDF segments in FE[19, 20], especially the peaks at 28.17° and 46.66°. The intensity of these two peaks are moderate, therefore the FE-72 is partially crystalline. Table 2 shows the peak list for FE-72 and FE-72T. Comparing FE and FE-72 in this table, it shows that the peaks increased in intensity especially at 28.17° and 46.66°. This shows that due to aging at high temperature, γ-phase crystallinity increase. As mentioned by Chae and Hong[10], at temperatures above 155°C, there is increasing γ-phase crystallinity.

Table 1. XRD peak list of FE and FE-T

FE					FE-T				
Pos. [°2θ]	Height [cts]	FWHM Left [°2θ]	Rel. Int. [%]	Tip Width	Pos. [°2θ]	Height [cts]	FWHM Left [°2θ]	Rel. Int. [%]	Tip Width
5.9633	17580.11	1.2280	57.22	1.4736	6.6402	15892.81	1.6374	60.01	1.9649
7.4599	18430.79	1.4327	59.99	1.7192	7.6846	15679.07	0.8187	59.21	0.9824
16.6266	30722.26	1.4327	100.00	1.7192	9.5119	14460.41	0.0768	54.60	0.0921
29.4540	11635.87	0.1023	37.87	0.1228	14.4596	19491.94	0.0768	73.60	0.0921
36.0843	6220.90	0.3070	20.25	0.3684	16.7321	26482.39	1.8420	100.00	2.2105
39.4710	6964.41	0.6140	22.67	0.7368	28.7223	5470.21	0.1535	20.66	0.1842
41.0552	6448.09	1.2280	20.99	1.4736	29.4914	9333.99	0.1279	35.25	0.1535
43.1614	5322.05	1.2280	17.32	1.4736	36.1282	6006.31	0.3070	22.68	0.3684
					39.1432	6627.46	6.1402	25.03	7.3682
					45.8451	3769.70	0.3070	14.23	0.3684

In Figure 5, for FE-72T, similar peaks as that of FE-72 appeared. However, the peak at 29.4° has higher intensity, and become sharper. Other peaks increased slightly. Table 2 also shows the peak list for FE-72T. Again, these results show that FE-72T is also partially crystalline and the crystallinity is in γ-phase form. The increase of relative intensity of the above mentioned common peaks and specifically the increase in the peak at 29.4° show that the crystallinity of FE-72T is slightly more than that of FE-72. Having new peaks with very low FWHM and tip width and considerable intensity also shows more crystallinity in FE-72T. Again the above results show that after tensile the crystallinity increases due to SIC. Once more, these results also confirm the tensile results that showed SIC during tensile test for FE.

Again, the amorphous hollows of FE-72T at 6.69° and 16.69° decreased compared to that of FE-72. It is due to increase in crystallinity due to SIC in FE-72T and decreasing amorphous part of FE. In Figure 5, comparison between FE-T and FE-72T show that the intensity of peaks at 28°, 64°, 29.42°, 39.22° and 47.08° increased. Relative intensity of common peaks in them also shows slightly more crystallinity in FE-72T. Once again these results show that due to aging at high temperature, γ-phase crystallinity increased. However, the peaks at 9.51° and 14.46° increased slightly in FE-T compared to FE-72T. Comparing the intensity of amorphous hollows of all four samples in Figure 5, it shows that the crystallinity intensity is in the order of FE-72T > FE-T > FE > FE-72. Therefore, SIC in tensile test samples increased the crystallinity compared to non-tensile test samples.

XRD of CB/FE Figure 6 shows XRD spectra of CB/FE and CB/FE-72 before and after tensile test. The figure shows a considerable peak for CB/FE at 29.45°, a peak at 39.31° and a few small peaks which are γ-phase crystallinity peaks. Table 3 shows the peak list for CB/FE. These peaks show that CB/FE is slightly crystalline and in γ-phase form.

An XRD spectra of CB/FE-T in the same figure shows many sharp and intense peaks. Table 3 also shows peak list of them. The high intensity and very sharp peaks show very high degree of crystallinity compared to that of CB/FE. A very low FWHM and tip width with high peaks indicate that the structure have very large crystals and is highly ordered. All of these peaks belonged to γ-phase[19–23] of VDF segments and TFE segments. Some peaks of VDF monomer are overlapped with peaks of TFE segments. The spectra of the TFE peaks were reported by Tieyuan et al.[25] Therefore, in CB/FE-T, γ-phase and TFE crystallinity segments increased considerably compared to CB/FE. In CB/FE-T, the amorphous hollows at 16.64° decreased and the one at 6.88° almost disappeared compared to CB/FE. This again shows the increase in crystallinity and decrease in amorphous portion. Once more, these results show that after tensile test, the crystallinity and crystal size increased to a great extent due to SIC.

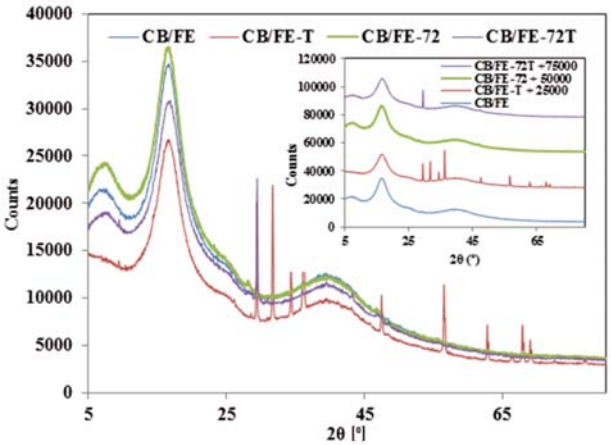

Figure 6. An XRD spectra of CB/FE and CB/FE-72 before and after tensile test (overlaid and separated)

Comparing CB/FE-T of Figure 6 and FE-T of Figure 5 shows that the SIC in the presence of CB is much more compared to unfilled FE. Figure 6 also shows that for CB/FE-72, there are some main peaks. The peak list for this figure is tabulated in Table 4. Similar to FE-72, all of these peaks show γ-phase crystallinity of VDF segments in FE, especially peaks at 28.13° and 46.76° are characteristic of γ-phase. Like FE-72, CB/FE-72 is partially crystalline. γ-phase crystallinity increased in CB/FE-72 in comparison to CB/FE. These results are the same as that of FE and FE-72. The peak at around 29.3° decreased in CB/FE-72 is probably due to aging at high temperature in the presence of CB compared to CB/FE.

In Figure 6, for CB/FE-72T, some of the peaks appeared are the same as that of CB/FE-T peaks. However, the smaller peaks of CB/FE-T did not appear in CB/FE-72T. The peak at 29.46° is sharp and intense. Table 4 also shows the peak list of CB/FE-72T. The above results show that CB/FE-72T is also partially crystalline and the crystallinity is in γ-phase form. The peaks especially at 28.25° and 47.54° are due to γ-phase. Similar to FE-72 and FE-72T, the crystallinity of CB/FE-72T is more than that of CB/FE-72. The new peaks in CB/FE-72T compared to CB/FE-72 has very low FWHM and tip width. The amorphous hollow appeared at 7.57° and 16.73° decreased in CB/FE-72T compared to CB/FE-72 indicates increase in crystallinity and decrease in amorphous portion.

Table 2. XRD peak list of FE-72 and FE-72T

FE-72					FE-72T				
Pos. [°2θ]	Height [cts]	FWHM Left [°2θ]	Rel. Int. [%]	Tip Width	Pos. [°2θ]	Height [cts]	FWHM Left [°2θ]	Rel. Int. [%]	Tip Width
5.9319	20509.41	0.8187	59.57	0.9824	6.6919	15257.79	1.8420	55.42	2.2105
7.1630	21458.28	2.0467	62.33	2.4561	14.4006	18200.94	0.1535	66.12	0.1842
16.5411	34428.24	2.0467	100.00	2.4561	16.6918	27528.97	1.1257	100.00	1.3508
28.1703	7472.34	0.5117	21.70	0.6140	29.0018	5754.45	0.1535	20.90	0.1842
39.2622	8527.58	2.2514	24.77	2.7017	29.4286	13166.24	0.1279	47.83	0.1535
42.1214	7454.00	2.0467	21.65	2.4561	39.3155	7237.23	1.6374	26.29	1.9649
46.7860	4879.88	0.5117	14.17	0.6140	42.2253	6078.87	2.0467	22.08	2.4561
55.5212	1665.44	1.2280	4.84	1.4736	47.0789	4009.30	0.2047	14.56	0.2456

Table 3. XRD peak list of CB/FE and CB/FE-T

CB/FE					CB/FE-T				
Pos. [°2θ]	Height [cts]	FWHM Left [°2θ]	Rel. Int. [%]	Tip Width	Pos. [°2θ]	Height [cts]	FWHM Left [°2θ]	Rel. Int. [%]	Tip Width
6.6402	15892.81	1.6374	60.01	1.9649	6.1345	11347.34	2.4561	42.51	2.9473
7.6846	15679.07	0.8187	59.21	0.9824	9.3912	10793.49	0.1535	40.44	0.1842
9.5119	14460.41	0.0768	54.60	0.0921	16.6367	23584.99	1.2280	88.36	1.4736
14.4596	19491.94	0.0768	73.60	0.0921	17.4084	21517.67	0.5117	80.62	0.6140
16.7321	26482.39	1.8420	100.00	2.2105	24.9809	7239.29	1.6374	27.12	1.9649
28.7223	5470.21	0.1535	20.66	0.1842	26.1235	6812.90	0.1535	25.53	0.1842
29.4914	9333.99	0.1279	35.25	0.1535	29.3956	17221.39	0.1023	64.52	0.1228
36.1282	6006.31	0.3070	22.68	0.3684	31.7095	18995.92	0.1279	71.17	0.1535
39.1432	6627.46	6.1402	25.03	7.3682	34.3642	11201.93	0.1023	41.97	0.1228
45.8451	3769.70	0.3070	14.23	0.3684	36.1950	26690.92	0.1535	100.00	0.1842
					39.3631	6730.78	3.2748	25.22	3.9297
					43.1504	5796.95	0.6140	21.72	0.7368
					47.4793	7327.55	0.1023	27.45	0.1228
					56.5266	8526.38	0.1248	31.94	0.1498
					56.7009	4649.37	0.0624	17.42	0.0749
					62.7965	4154.54	0.0936	15.57	0.1123
					62.9637	2372.57	0.0936	8.89	0.1123
					66.3063	1283.19	0.1248	4.81	0.1498
					67.8837	4153.92	0.1248	15.56	0.1498
					68.0889	2305.54	0.0624	8.64	0.0749
					69.0186	2579.34	0.0936	9.66	0.1123
					69.2086	1468.91	0.0936	5.50	0.1123
					72.5615	284.64	0.3744	1.07	0.4493
					76.8946	619.94	0.0936	2.32	0.1123

Table 4. XRD peak list of CB/FE-72 and CB/FE-72T

CB/FE-72					CB/FE-72T				
Pos. [°2θ]	Height [cts]	FWHM Left [°2θ]	Rel. Int. [%]	Tip Width	Pos. [°2θ]	Height [cts]	FWHM Left [°2θ]	Rel. Int. [%]	Tip Width
6.1259	19496.08	1.0234	60.13	1.2280	7.5715	14999.44	1.6374	56.03	1.9649
7.3389	20237.82	0.7164	62.42	0.8596	9.4618	14380.04	0.0768	53.71	0.0921
15.6729	29441.39	0.7164	90.81	0.8596	16.7273	26772.52	1.4327	100.00	1.7192
16.5432	32420.79	0.9210	100.00	1.1052	25.5737	8498.00	0.9210	31.74	1.1052
25.2695	9809.72	2.0467	30.26	2.4561	28.2500	6731.50	0.4093	25.14	0.4912
28.1276	7816.60	0.3070	24.11	0.3684	29.4621	18641.46	0.1279	69.63	0.1535
39.5827	8214.34	1.2280	25.34	1.4736	30.9926	6011.51	0.1535	22.45	0.1842
42.8146	6987.13	2.4561	21.55	2.9473	39.4943	7680.51	0.3070	28.69	0.3684
46.7646	4819.12	0.5117	14.86	0.6140	43.2248	6502.88	0.2047	24.29	0.2456
55.6646	1685.61	0.6140	5.20	0.7368	47.5493	4268.30	0.1535	15.94	0.1842
					48.5309	3541.39	0.2047	13.23	0.2456

In Figure 6, comparing CB/FE-T and CB/FE-72T shows that the intensive and sharp peaks of CB/FE-T changed to small peaks for CB/FE-72T, except the peak at 29.46°. These results indicate that due to aging at high temperature in the presence of CB, the crystallinity of tensile tested elastomer is reduced sensibly. Once again, comparing the intensity of the amorphous hollows of all four samples in Figure 6 indicates that the crystalline intensity is as follows: CB/FE-T > CB/FE-72T > CB/FE > CB/FE-72. Therefore, SIC in tensile test samples increased the crystallinity compared to non-tensile test samples.

XRD of CNT/FE Figure 7 shows XRD spectra of CNT/FE and CNT/FE-72 before and after tensile test. Table 5 shows the peak list for CNT/FE. These results show that CNT/FE is slightly crystalline and the crystallinity is in γ-phase form, the reasons are the same as those mentioned for CB/FE. The peaks at 26.02° and 26.28° are the overlapped peaks of CNT[16] and γ-phase peak[19].

CNT/FE-T XRD spectra presented in the same figure and Table 5 shows the peak list of it. Again, based on these results, CNT/FE-T and CNT/FE shows the same properties that CB/FE-T and CB/FE do. CNT/FE-T shows very high degree of crystallinity and highly ordered large crystals. These results show that the degree of

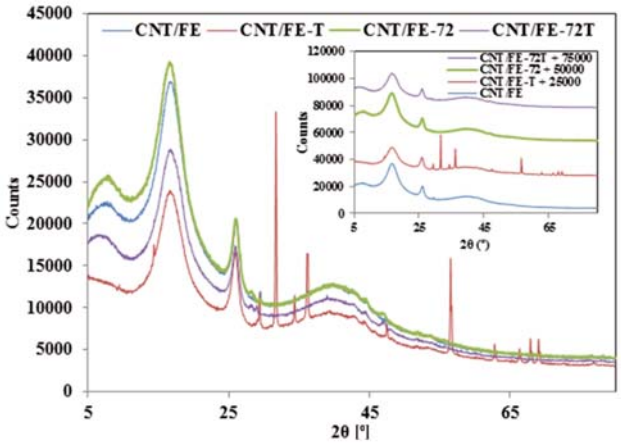

Figure 7. An XRD spectra of CNT/FE and CNT/FE-72 before and after tensile test (overlaid and separated)

crystallinity increases with SIC in the presence of CNT. Comparing CNT/FE-T and CNT/FE of Figure 7 indicates that the SIC in CNT/FE-T is considerably higher. Figure 7 also shows that for CNT/FE-72, there are new peaks at 28.18°, 46.88° and 53.60°. The peak list is presented in Table 6. All of these peaks show γ-phase crystallinity with considerable intensity which indicates partial

Table 5. XRD peak list of CNT/FE and CNT/FE-T

CNT/FE					CNT/FE-T				
Pos. [°2θ]	Height [cts]	FWHM Left [°2θ]	Rel. Int. [%]	Tip Width	Pos. [°2θ]	Height [cts]	FWHM Left [°2θ]	Rel. Int. [%]	Tip Width
7.5435	18117.89	1.8420	55.46	2.2105	14.3605	14335.27	0.0768	47.17	0.0921
16.7333	32667.22	2.0467	100.00	2.4561	16.6636	20709.47	1.9444	68.15	2.3333
26.0174	16115.57	0.3070	49.33	0.3684	25.9181	13320.50	0.7675	43.83	0.9210
26.2798	15321.18	0.2047	46.90	0.2456	29.3762	8631.16	0.1279	28.40	0.1535
29.4754	7762.76	0.1279	23.76	0.1535	31.6985	30389.63	0.1279	100.00	0.1535
39.6843	8512.91	0.6140	26.06	0.7368	34.3474	8279.77	0.1279	27.25	0.1535
42.9767	7575.57	0.6140	23.19	0.7368	36.1779	20132.82	0.1535	66.25	0.1842
44.6300	6495.15	0.4093	19.88	0.4912	39.2850	6397.88	0.8187	21.05	0.9824
45.9473	5221.49	0.3070	15.98	0.3684	42.7305	5848.60	0.8187	19.25	0.9824
53.6761	2409.06	0.8187	7.37	0.9824	44.2676	5169.91	0.4093	17.01	0.4912
					47.4648	5015.24	0.1279	16.50	0.1535
					53.2158	2115.18	0.6140	6.96	0.7368
					56.5192	12759.13	0.1248	41.99	0.1498
					56.6863	6875.02	0.0936	22.62	0.1123
					62.7775	2495.84	0.0936	8.21	0.1123
					66.3065	2009.33	0.0936	6.61	0.1123
					67.8663	3153.49	0.1248	10.38	0.1498
					68.0552	1620.74	0.0936	5.33	0.1123
					69.0089	3140.91	0.1248	10.34	0.1498
					69.1981	1650.45	0.0936	5.43	0.1123
					76.8753	590.10	0.0936	1.94	0.1123

crystallinity. The peak at 53.60° is also probably due to γ-phase crystallinity. Due to high temperature, γ-phase crystallinity increased in CNT/FE-72 compared to CNT/FE. The results are the same as that of FE and CB/FE.

Figure 7 show XRD spectra of CNT/FE-72T too. Table 6 also shows the peak list for CNT/FE-72T. Based on these results and similar to CB/FE-72 and CB/FE-72T, the following conclusios can be made: CNT/FE-72T is slightly crystalline in the form of γ-phase, especially the peaks at 28.18°, 28.98°, 46.96° and 53.89° are indicative of γ-phase. The crystallinity degree in CNT/FE-72T slightly increased and amorphous parts decreased compared to CNT/FE-72. CNT/FE-72T has crystals with less size compared to CNT/FE-T. Comparison of CNT/FE-T and CNT/FE-72T again shows that due to aging at high temperature in the presence of CNT too, the crystallinity of stretched elastomer reduced significantly.

The comparison of amorphous hollows of all samples shows that the degree of crystallinity has the following order among the samples: CNT/FE-T > CNT/FE-72T > CNT/FE > CNT/FE-72 which is the same trend as CB/FE. This order shows that SIC increased the crystallinity for CNT/FE. Shear field (high shear mixing during compounding and molding) promotes the formation of polar γ-crystalline phase.

Figure 8 shows the FESEM images of CNT/FE (the razor cut cross section surface) and CB/FE-48. The very good distribution and dispersion of CNT and CB in FE can be seen in this figure.

Verifying crystalinity and studying chemical degradation In our before study[26], we verified the crystalinity of some of the above mentioned FE and fillers/FE, by Dynamic Mechanical Analysis (DMA), Differential Scanning Calorimetry (DSC) and X-ray diffraction (XRD). In addition in another study[27], for the before mentioned FE and fillers/FE, we revealed the effect of heat aging on chemical degradation by Energy Dispersive X-Ray (EDX). Verifying thermal properties of fluoroelastomer using carbon nanotubes in presence of air and under nitrogen flow is the other study[28].

Table 6. XRD peak list of CNT/FE-72 and CNT/FE-72T

CNT/FE-72					CNT/FE-72T				
Pos. [°2θ]	Height [cts]	FWHM Left [°2θ]	Rel. Int. [%]	Tip Width	Pos. [°2θ]	Height [cts]	FWHM Left [°2θ]	Rel. Int. [%]	Tip Width
6.1684	20004.89	1.2280	57.47	1.4736	6.5253	14828.97	1.4327	59.39	1.7192
7.6807	21123.57	1.4327	60.69	1.7192	7.7059	14579.13	0.8187	58.39	0.9824
16.6414	34806.38	1.8420	100.00	2.2105	16.6800	24969.72	1.1257	100.00	1.3508
26.0048	16299.59	0.7164	46.83	0.8596	17.9897	21180.32	0.6140	84.82	0.7368
26.6576	11860.57	0.0768	34.08	0.0921	25.9566	13298.05	0.5117	53.26	0.6140
28.1823	7608.46	0.4093	21.86	0.4912	28.1842	6444.93	0.3070	25.81	0.3684
39.7215	8419.32	4.9121	24.19	5.8946	28.9777	6414.38	0.2047	25.69	0.2456
42.9086	7558.15	0.8187	21.71	0.9824	39.1045	7350.81	0.6140	29.44	0.7368
44.5437	6628.75	0.4093	19.04	0.4912	42.7602	6626.04	0.6140	26.54	0.7368
46.8803	5003.85	0.6140	14.38	0.7368	44.3330	5666.57	0.5117	22.69	0.6140
51.9204	2740.42	0.6140	7.87	0.7368	46.9559	4472.47	0.5117	17.91	0.6140
53.5991	2396.27	0.6140	6.88	0.7368	53.8893	2042.53	1.2280	8.18	1.4736

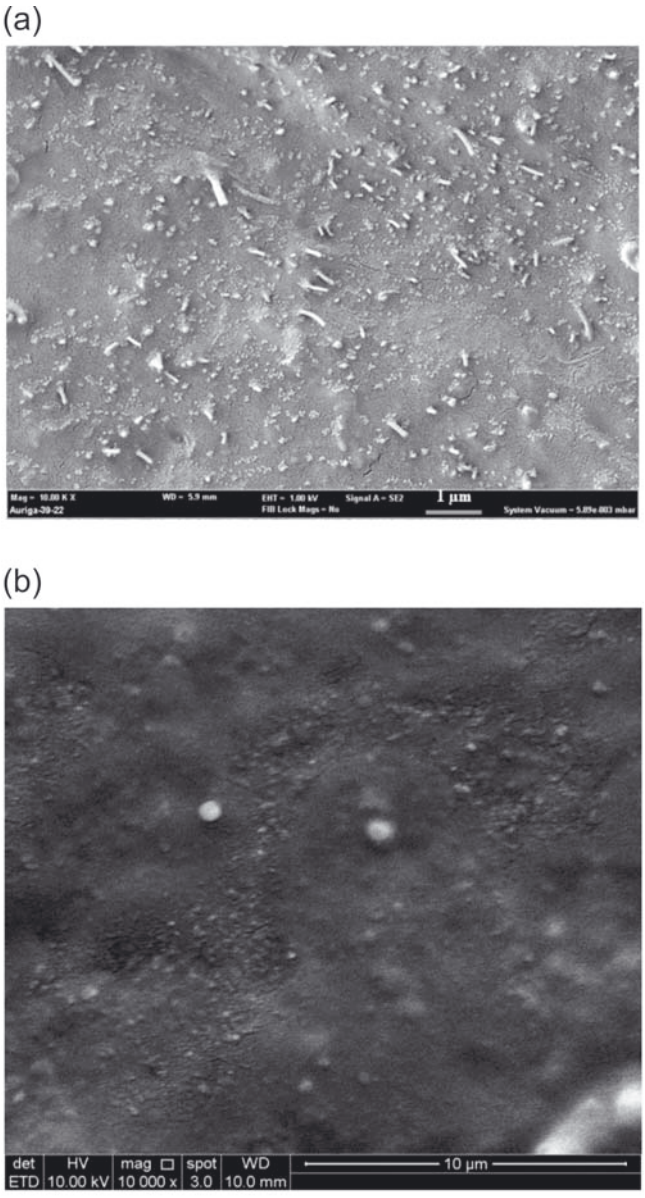

Figure 8. FESEM images of (a) CNT/FE (the razor cut cross section surface) and (b) CB/FE-48

CONCLUSIONS

Comparing tensile properties of unaged and heat air aged FE, CB/FE and CNT/FE show that CNT improved tensile properties of FE before and after aging. The increase in NM and TM at fixed strain for aged and un-aged FE composites are in the order of CNT/FE > CB/FE > FE. TS has the order of CNT/FE > CB/FE > FE, while EB has the reverse order: FE > CB/FE > CNT/FE. All samples show SIC in the stress-strain curves; in FE, CB/FE and CNT/FE the strain started at 200%, 100% and 25% respectively. XRD results indicate that FE, CB/FE and CNT/FE are in γ-phase form before and after aging (original compound). Un-aged specimens that undergo tensile testing displayed this characteristic as well before and after the test. The tensile tested, aged specimens were also in γ-phase form. However, the degree of crystallinity is dependent on the conditions. TFE crystalline peaks were also observed. Non-aging or aging alone causes slight crystallinity with low crystal size. Tensile test alone increases the degree of crystallinity and crystal size considerably in non-aged CB/FE, CNT/FE and FE samples. Tensile test also proves that aged samples have less degree of crystallinity after testing compared to non-aged samples. XRD results confirm tensile results which shows SIC after tensile test.

ACKNOWLEDGEMENTS

We thank the University of Malaya as the work reported in this paper was funded under the grant numbers FRGS (FP021-2013A) and BKP (BK005-2014).

LITERATURE CITED

1. Endo, M., Noguchi, T., Ito, M., Takeuchi, K., Hayashi, T., Kim, Y.A., Wanibuchi, T., Jinnai, H., Terrones, M. & Dresselhaus, M.S. (2008). Extreme-performance rubber nanocomposites for probing and excavating deep oil resources using multi-walled carbon nanotubes. *Adv. Func. Mat. 18*, 3403–3409. DOI: 10.1002/adfm.200801136.

2. Noguchi, T., Ueki, H., Inukai, S., Iinou, S. & Ito, M. (2011). U.S Patent No. 2011/0160375. Washington, D.C.: U.S. Patent and Trademark Office.

3. Ito, M., Noguchi, T., Ueki, H., Takeuchi, K. & Endo, M. (2011). Carbon nanotube enables quantum leap in oil recovery. *Mater. Res. Bull. 46*, 1480–1484. DOI: 10.1016/j.materresbull.2011.04.028.

4. Faulkner, W.R. , Mumby, K.J., Fischer, A., Jozokos, T. & Zhou, S. (2009). Multiwall carbon nanotube reinforcement of HNBR and FKM. Proc. of the Fall 176th Technical meeting of the rubber division, Pittsburgh, PA, USA, 13–15 Oct.

5. Wang, Y., Liu, L., Luo, Y. & Jia, D. (2009). Aging behavior and thermal degradation of fluoroelastomer reactive blends with poly-phenol hydroxy EPDM. *Polym. Degrad. Stab. 94*, 443–449. DOI: 10.1016/j.polymdegradstab.2008.11.007.

6. Smith, G., Park, D., Titchener, K., Davies, R. & West, R. (1995). Surface studies of oil-seal degradation. *Appl. Surf. Sci. 90*, 357–371. DOI: 10.1016/0169-4332(95)00165-4.

7. Mago, G., Fisher, F.T. & Kalyon, D.M. (2009). Deformation-induced crystallization and associated morphology development of carbon nanotube-PVDF nanocomposites. *J. Nanosci. Nanotechnol. 9*, 3330–3340. DOI: http://dx.doi.org/10.1166/jnn.2009.VC08

8. Huang, S., Yee, W.A., Tjiu, W.C., Liu, Y., Kotaki, M., Boey, Y.C.F., Ma, J., Liu, T. & Lu, X. (2008). Electrospinning of polyvinylidene difluoride with carbon nanotubes: synergistic effects of extensional force and interfacial interaction on crystalline structures. *Langmuir 24*, 13621–13626. DOI: 10.1021/la8024183.

9. Maiti, M. & Bhowmick, A.K. (2007). Dynamic viscoelastic properties of fluoroelastomer/clay nanocomposites. *Polym. Eng. Sci. 47*, 1777–1787. DOI: 10.1002/pen.20877.

10. Chae, D.W. & Hong, S.M. (2011). Rheology, crystallization behavior under shear, and resultant morphology of PVDF/multiwalled carbon nanotube composites. *Macromol. Res. 19*, 326–331. DOI: 10.1007/s13233-011-0403-1.

11. Yang, J., Wang, J., Zhang, Q., Chen, F., Deng, H., Wang, K. & Fu, Q. (2011). Cooperative effect of shear and nanoclay on the formation of polar phase in poly (vinylidene fluoride) and the resultant properties. *Polymer 52*, 4970–4978. DOI: 10.1016/j.polymer.2011.08.051.

12. Buckley, J., Cebe, P., Cherdack, D., Crawford, J., Ince, B.S., Jenkins, M., Pan, J., Reveley, M., Washington, N. & Wolchover, N. (2006). Nanocomposites of poly(vinylidene fluoride) with organically modified silicate. *Polymer 47*, 2411–2422. DOI: http://dx.doi.org/10.1016/j.polymer.2006.02.012

13. Andrew, J.S. & Clarke, D.R. (2008). Effect of electrospinning on the ferroelectric phase content of polyvinylidene difluoride fibers. *Langmuir 24*, 670–672. DOI: 10.1021/la7035407.

14. Huang, F., Wei, Q., Wang, J., Cai, Y. & Huang, Y. (2008). Effect of temperature on structure, morphology and crystallinity of PVDF nanofibers via electrospinning. *e-Polym* 8, 1758. DOI: 10.1515/epoly.2008.8.1.1758.

15. Yee, W.A., Nguyen, A.C., Lee, P.S., Kotaki, M., Liu, Y., Tan, B.T., Mhaisalkar, S. & Lu, X. (2008). Stress-induced structural changes in electrospun polyvinylidene difluoride nanofibers collected using a modified rotating disk. *Polymer 49*, 4196–4203. DOI: http://dx.doi.org/10.1016/j.polymer.2008.07.032

16. Pham, T.T., Sridhar, V. & Kim, J.K. (2009). Fluoroelastomer-MWNT nanocomposites-1: Dispersion, morphology, physico-mechanical, and thermal properties. *Polym. Compos. 30*, 121–130. DOI: 10.1002/pc.20521.

17. Shanmugharaj, A., Bae, J., Lee, K.Y., Noh, W.H., Lee, S.H. & Ryu, S.H. (2007). Physical and chemical characteristics of multiwalled carbon nanotubes functionalized with aminosilane and its influence on the properties of natural rubber composites. *Compos. Sci. Technol. 67*, 1813–1822. DOI: 10.1016/j.compscitech.2006.10.021.

18. Freimuth, H., Sinn, C. & Dettenamaier, M. (1996). Structure and deformation behaviour of a vinylidene fluoride—tetrafluoroethylene— hexafluoropropylene terpolymer. *Polymer 37*, 831–836. DOI: http://dx.doi.org/10.1016/0032-3861(96)87261-2

19. Satapathy, S., Pawar, S., Gupta, P. & Varma, K. (2011). Effect of annealing on the phase transition in poly (vinylidene fluoride) films prepared using polar solvent. *Bull. Mater. Sci. 34*, 727–733. DOI: http://dx.doi.org/10.1007/s12034-011-0187-0

20. Elashmawi, I. (2008). Effect of LiCl filler on the structure and morphology of PVDF films. *Mater. Chem. Phys. 107*, 96–100. DOI: 10.1016/j.matchemphys.2007.06.045.

21. Gao, K., Hu, X., Dai, C. & Yi, T. (2006). Crystal structures of electrospun PVDF membranes and its separator application for rechargeable lithium metal cells. *Mater. Sci. Eng. B 131*, 100–105. DOI: 10.1016/j.mseb.2006.03.035.

22. Rana, D.S., Chaturvedi, D. & Quamara, J. (2009). Morphology, crystalline structure, and chemical properties of 100 MeV Ag-ion beam irradiated polyvinylidene fluoride (PVDF) thin film. *J. Optoelectron. Adv. M. 11*, 705–712.

23. Ozkazanc, E., Guney, H.Y., Guner, S. & Abaci, U. (2010). Morphological and dielectric properties of barium chloride-filled poly (vinylidene fluoride) films. *Polym. Compos. 31*, 1782–1789. DOI: 10.1002/pc.20970.

24. Sajkiewicz, P. (1999). Crystallization behaviour of poly (vinylidene fluoride). *Eur. Polym. J. 35*, 1581–1590. DOI: 10.1016/S0014-3057(98)00242-0.

25. Tieyuan, F., Zhishen, M., Ping, H., Yuchen, Q., Shuyun, W. & Donglin, C. (1986). Study on factors affecting room temperature transition of polytetrafluoroethylene. *Chin. J. Polym. Sci. (CJPS) 4*, 170–179.

26. Heidarian, J. & Hassan, A. (2014). Microstructural and thermal properties of fluoroelastomer/carbon nanotube composites. *Compos. Part B-Eng.* 58, 166–174. DOI: http://dx.doi.org/10.1016/j.compositesb.2013.10.054

27. Heidarian, J., Hassan, A. & Normasmira, A.R. (2015). Improving the thermal properties of fluoroelastomer (Viton GF-600S) using acidic surface modified carbon nanotube. *Polímeros 25*(4), 392–401. DOI: 10.1080/09276440.2016.1127668.

28. Heidarian, J. & Hassan, A. (2015). Improving thermal properties of fluoroelastomer using carbon nanotubes in presence of air and under nitrogen flow. *Asian J. Chem.* 27, 1235. DOI: http://dx.doi.org/10.14233/ajchem.2015.17200